Nuclear Instruments and Methods in Physics Research B 88 (1994) 355–364
North-Holland

NIM B
Beam Interactions with Materials & Atoms

Simulation of the primary stage of the interaction of swift heavy ions with condensed matter

Benoit Gervais and Serge Bouffard *
CIRIL, laboratoire mixte CEA-CNRS, Rue Claude Bloch, B.P. 5133, 14040 Caen Cedex, France

Received 3 December 1993 and in revised form 1 March 1994

In this paper the swift heavy ion interactions with condensed matter are studied from the point of view of the modifications induced in the electronic subsystem of the target. A Monte Carlo method is used to describe event by event the interactions of the projectile with the target electrons as well as the evolution of the electronic subsystem. The validity of the method and the results are discussed. This detailed picture of the excited target could be used for further explanations and calculations of the damage creation by electronic excitation. We have focused our attention on two materials whose electronic properties are different: graphite and quartz. For both materials a quantitative analysis of the energy deposition mechanism is given.

1. Introduction

Initially, only the atomic physics has studied the interaction of swift heavy ions with condensed matter. Thus many theoretical and experimental studies have been done on the interaction cross sections [1–3] and on the ion slowing down [4–8]. More recently the response of the target to the energy loss of swift heavy ions has been investigated experimentally. Since the sixties, nuclear etched tracks were observed and used for registration of fast heavy particles [9–11]. Much later, the defects giving the possibility for the etching process (latent tracks), were studied by X-ray diffraction [12,13]. Finally the GeV ion beam facilities allow a more detailed investigation of the track structure in insulators [14,15] and the observation of new phenomena which cannot be predicted by classical models of damage production. The most spectacular effects are the damage creation by electronic excitations in metallic and non-metallic conductors [16–21] and the anisotropic growth of amorphous solids [22,23]. In every case the damage is related to the dense excitation along the ion path. Indeed in the energy range considered here (greater than 1 MeV/amu), the electronic stopping power could reach values as high as a few tenths of keV/nm, and we will show hereafter that such an ion could produce several ionisations per interatomic distance.

Several models have been proposed to explain the damage track creation via electronic excitations. The first one is the thermal spike model introduced by Seitz and Koehler [24] and recently revisited by Toulemonde et al. [25,26]. In this model, the temperature of the electronic subsystem is locally increased along the ion path. Through the electron–phonon coupling the lattice could be sufficiently heated up to induce a phase transformation which must be quenched. In the second model, namely the Coulomb explosion, the electron–hole separation due to electron ejection around the ion path induces an electric field which could produce an incoherent [10] or coherent [27] movement of the target atoms.

To be predictive, both of these approaches need the knowledge of the initial conditions a short time after the ion interaction. Unfortunately, the time and distances involved in the spread out of the energy are too small ($<$ ps and $\sim$ nm), so the only way to measure this energy distribution around the ion path consists in extrapolating the measurements in gas [28,29] to the case of dense target. But doing so, we suppose that the collective response does not play any role. An alternative approach is the simulation by an adapted code of the relaxation of the electronic energy. Such distributions of the dose around the ion path have been studied either to describe the response of particle detectors [30,31] or to understand the behaviour of biological systems under ion irradiation [32–35].

In this paper we present a simulation of the spread-out of the energy around the ion path by a Monte Carlo (MC) code. This is a classical way to describe multi-event phenomena, where each event may be successively tossed at random [36]. The probability of one

* Corresponding author, tel. +33 31454613, fax +33 31454714, e-mail bouffard@ganac4.in2p3.fr.

SSDI 0168-583X(94)00166-S

event depends on its cross section relative to the total cross section of interaction. Thus in our case, we have to know the doubly differential cross sections with respect to the transferred energy and to the angle of emission for ion–solid and electron–solid interactions.

In section 2 we present the calculation method and the schematic electronic structure we have adopted to describe the target material. In section 3 we discuss our choice of the ion–solid interaction cross sections, and in section 4 the transport of the electrons and their contribution to the modification of the energy distribution. Finally, in section 5 we present some results on microdosimetry and on the density of ionisation around a track of a single ion. We also discuss the limits of such an approach and the validity of these results regarding the method and the inaccuracy of the used cross sections.

2. Calculation

In order that the code should be usable for many kinds of material, we describe the material in a simplified way. First we consider the material as an homogeneous and an isotropic medium. Secondly, the density of electronic states is divided into two parts: the core levels which are regarded as atomic levels with eventually some shifts in energy due to solid effects, and the valence electrons which are described with more details. The best description of the valence and conduction bands should be extracted from the dielectric response of the solid. However such a calculation rapidly becomes intractable. So we have chosen to use the following assumptions: For insulators, only the density of states of the valence band and the energy gap are taken into account. The valence levels for which the electrons are assumed to be localised on a site are regarded as atomic levels. Thus the coherent collective motion of the electrons is neglected. It is a fairly good approximation because these collective coherent excitations are strongly damped in insulators [37], and they could be regarded as a succession of incoherent independent interactions. At the opposite, for semiconductors and conductors, the energy loss by plasmon excitations is explicitly taken into account by means of the dielectric response theory of a free electron gas [38,39]. For conductors, the following relation gives the relation between the plasma frequency and the density of the valence electrons n:

$$\omega_0^2 = \frac{4\pi n e^2}{m}, \tag{1}$$

where e and m are respectively the charge and the mass of an electron, while for semiconductors the presence of the gap modifies the plasma frequency as follows [40]:

$$\omega_0^2 = \frac{4\pi n e^2}{m} + \frac{E_g^2}{\hbar^2} \tag{2}$$

where E_g is the energy gap.

For these materials, a free electron gas density of states is assumed. This approximation modifies only the low energy transfer and not the spatial distribution.

In the next sections, we shall not consider explicitly the excitation cross section because ionisations and excitations are very similar in solid target. For both processes, the active electron makes a transition from its fundamental state to a delocalized state in the conduction band. Thus the electron in the final state can be regarded as free, and we choose the origin of the kinetic energy at the first free level.

For the target described above, the electron–ion interactions and the diffusion of the knocked electrons are described in a stochastic way. The probability of each event is directly deduced from its relative cross section. In addition the MC method assumes classical trajectories for particles, and then a criterion of validity is deduced from the Heisenberg uncertainty principle. The De Broglie wavelength λ of the particle must be smaller than the characteristic atomic size. λ is related to the kinetic energy E by the following relations:

$$\lambda \sim \frac{5 \times 10^{-2}}{\sqrt{E}} \qquad \text{for ions,} \tag{3}$$

$$\lambda \sim \frac{2}{\sqrt{E}} \qquad \text{for electrons,} \tag{4}$$

where E and λ are expressed respectively in eV and in Å. So the condition is fulfilled for the ions in the MeV to GeV range. But for electrons, E must be greater than 100 eV to neglect the quantum effects. However, as a first approximation this classical treatment is used even at low energy.

The calculation could be summarised as follows: First we toss up an interaction type between the projectile and the target electrons: plasmon emission or target ionisation. For every interaction we toss up the energy and the momentum exchange q between the projectile and the target using the differential cross section, and from the classical laws of electrostatic, we deduce the impact parameter b:

$$b = \frac{2\alpha Z}{\beta q}. \tag{5}$$

α, β and Z are respectively the fine structure constant, the relative velocity, and the charge of the projectile. For these primary ionisations, the estimation of b gives us the hole distributions. In the case of plasmon cre-

ation, we must determine where and when the decay occurs. The plasmon lifetime τ is deduced from optical measurement of the dielectric response function. Using the Poisson law the probability p of de-excitation per unit time is

$$p(t) = \Gamma\, e^{-\Gamma t} \quad \text{with } \Gamma = 1/t, \tag{6}$$

from which we obtain a random lifetime t and the diffusion length $l = vt$, where v is the plasmon group velocity. Plasmon decay should lead to the creation of several electron–hole pairs by interband transition [41,42], but for the simplified scheme we assume here, plasmon decay leads to only one electron–hole creation with the plasmon energy.

Following step by step every primary and secondary electron, we calculate explicitly the electronic cascade evolution. A cutoff energy – typically a tenth of eV – and a cutoff time are selected to stop the computation. Every interaction of the knocked electron with the target is taken into account. The ionisation energy, the energy transferred during the elastic collision between the electron and the nucleus, and the residual kinetic energy when the electron reaches the cutoff value are stored in different histograms which give the different events and dose distribution around the ion path. For a plasmon created by the electron, the energy is transported during the plasmon lifetime randomly chosen, as described above. For the times we consider here, which are much smaller than the characteristic time of lattice vibration – $\sim 10^{-13}$ s – the elastic energy does not diffuse throughout the lattice.

For this first calculation, we choose to neglect the Auger process and the fluorescence [43–45] which could carry away the energy in a time scale of the order of 10^{-15} s. It is difficult to take into account these processes because in the wake of swift heavy ions, the target atoms are often multi-ionised, and the competition between radiative and non-radiative processes could be slightly modified.

3. Ion–solid interaction

To evaluate the energy distribution around the ion path, we are only interested in the target and not in the projectile modification. The projectile is considered as a point charge at equilibrium. Therefore, neglecting the charge state fluctuations due to captures and ionisations, we adopt the effective charge state given by the Barkas formulae [46]:

$$Z_{\text{eff}} = Z_P\left[1 - \exp\left(-125\beta Z_P^{-2/3}\right)\right], \tag{7}$$

where Z_P is the atomic number and β the relative velocity of the projectile. This charge is not the actual mean charge of the projectile inside the solid, but the one which gives the "correct value" of the stopping power. Z_{eff} can be slightly different from the charge state measured by a beam foil experiment [47]. So this parameter can be seen as an adjustable parameter which includes the modification of the charge state and the screening induced by the dynamical response of the valence electrons. Any surface is also considered to be far away from the interaction point.

Moreover, the ion energy is kept constant and the angular scattering of the projectile is negligible. The elastic collisions which induce the largest angular diffusion do not contribute significantly to the stopping power at the considered energy. Therefore we assume that the ion travels along a straight line, and a cylindrical geometry is adopted.

As discussed previously, the core levels are treated as atomic levels. The ionisation cross section has been calculated by Khandelwahl and Merzbacher [48,49] using hydrogenic wave functions in the framework of the first Born approximation. They give the doubly differential cross section with respect to the energy loss and the transferred momentum. The azimuthal emission angle of the active electron is determined in a classical way from the momentum conservation law for a two body collision. The initial velocity of the electron is tossed up at random in direction and in magnitude within a range related to the considered level. The polar angle is chosen at random between 0 ant 2π using a uniform distribution law. For the valence band of insulators, the probability of interaction with a given level of energy U may be derived as follows: The cross section $\sigma(U)$ of interaction with an electron with energy U is calculated as for the core levels, but the interaction probability is balanced by the density of states at the energy U. The results we obtain for the interaction between Ne at 10 MeV/amu and quartz are summarised in Table 1.

For conductors and semiconductors, the interactions with the valence electrons are described using an

Table 1
The relative contributions of the different levels to the inverse mean free path λ^{-1} and to the electronic stopping power $\partial E/\partial x$ in the case of 10 MeV/amu Ne into quartz. N is the number of electrons in a given level per unit of SiO_2, and U is the ionization energy

Level	N	U [eV]	λ^{-1} [nm^{-1}]	$\partial E/\partial x$ [eV nm^{-1}]
valence	12	~14	8.58	610
$2s_O$	4	30	1.01	110
$2p_{Si}$	6	108	0.43	190
$2s_{Si}$	2	158	9.2×10^{-2}	50
$1s_O$	4	538	6.1×10^{-2}	110
$1s_{Si}$	2	1848	6×10^{-3}	30
total	30		10.18	1100

Table 2
The relative contributions of the different possibility of interactions to the inverse mean free path λ^{-} and to the electronic stopping power $\partial E/\partial x$ for 10 MeV/amu Ne into graphite

Level	N	U [eV]	λ^{-1} [nm^{-1}]	$\partial E/\partial x$ [eV nm^{-1}]
pair	4	~12	3.69	430
plasmon	4	25	11.52	300
1s	2	284	0.23	230
total	6		15.45	960

expression given by Ritchie and Anderson [39] for the doubly differential inverse mean free path λ^{-1}:

$$\frac{\partial^2\lambda^{-1}}{\partial\omega\partial q} = \frac{2Z^2e^2}{\pi\hbar v^2 q}\left[\frac{1}{\epsilon(\omega, q)}\right], \tag{8}$$

where $\hbar\omega$ and $\hbar q$ are respectively the energy and the momentum exchanges. $\epsilon(\omega,q)$ is the Lindhard dielectric function [38], which depends on the electron gas density. The doubly differential inverse mean free path must be integrated over the momentum and the energy to obtain the inverse mean free path or the probability of interaction per unit length. The limits of integration are given by the classical laws of the energy and the momentum conservation. Of course, the gap of the semiconductors introduces a difference between conductors and semiconductors by modifying the lower energy limit of integration. The results for graphite are reported in Table 2 and we note that the plasmon creation amounts to 30% of the energy loss and that this low energy transfer (25 eV) reduces the mean free path (0.065 nm for graphite compared to 0.1 nm for the insulator quartz for the same projectile Ne 10 MeV/amu).

4. Electron–solid interaction cross section

The interaction of electrons with the solid is similar to the ion–solid interaction in many respects, because the electron as any charged particle obeys the same electrodynamical laws. However, the lighter mass of the electron induces some differences.

The first one, as shown previously, is the nonclassical behaviour for the low energies. The second one comes from the relative importance of the elastic collisions. Such collisions do not contribute significantly to the energy loss of the electron, but they dominate its angular deflections. In fact, for low energy electrons, the angular differential cross section becomes almost isotropic. Thus, a low energy electron suffers a walk at random and loses its residual kinetic energy inside a small volume. Only the energy could diffuse by energy exchange between the particles, particularly for metals in which the diffusivity is high [50] ($D \sim 4$ to 150 cm^2/s in Cu between 10^4 and 300 K). Therefore we store the energy at the current location when the residual kinetic energy of the electron reaches the cutoff value. As long as we are interested in short time (smaller than 10^{-15} s), we do not introduce a large error in the dose distribution. For longer times, the low energy processes should include the electron–phonon interactions, which are not the aim of this work. Thus in our approach we consider only a static lattice, because the characteristic time of the lattice vibration – $\sim 10^{-13}$ s – is much larger that the cutoff time.

At low energy the first Born approximation does no longer work, so we use the phase shift analysis to calculate the elastic cross section. The interaction potential is described by a Thomas–Fermi central screening potential due to Molière [51], which only depends on the atomic number of the target. For polyatomic target the cross section of each component is calculated. For the sake of simplicity, the distribution of azimuthal angle is obtained in the framework of the first Born approximation, giving a more simple analytical formula than the phase shift analysis. We have previously compared both expressions and found that they give very close values. Moreover, they yield the same mean value, whatever the energy is.

For the inelastic collisions between the electron and the target, we follow the same target description as for the ion–solid interactions. But for the core levels and the insulator valence levels, the computer time consuming Born cross section is replaced by the cross section of binary encounter given by Gryzinski [52]. In this approach an analytical expression is proposed for the total and single differential cross section, which only depends on the ionisation energy of the level. The angular diffusion is treated using the binary encounter theory. As for ions, the valence band of conductors and semiconductors is described using the dielectric theory with a different kinematic limit, due to a difference in the projectile mass.

5. Results and discussion

With the MC calculation described above, we are able to obtain the distribution in space and time of the deposited energy density, or the hole density level by level, and the distribution function of the electrons in the phase space. Such quantities are of great interest for the damage creation models which need a local description of the material immediately after the ion passage [26,18].

Two materials are chosen as examples, a conductor, graphite, which is a low Z semi-metal, the electronic properties of which are well described, and an insula-

tor, quartz, whose behaviour under irradiation is well known [53]. The first results we shall discuss concern the radial deposition of the energy for two ions and for two energies and we compare them with the results of other authors [33,34,54]. We shall also describe the effect of plasmon creation on the dissipation of the energy in the graphite. Afterwards, we shall discuss the accuracy of the calculation for high density of ionisations due to very strong perturbations. Finally the time dependence of the space charge and of the energy density will be given.

As far as the microdosimetry is concerned, the results are displayed in Figs. 1 and 2. In Fig. 1 the radial distribution of the deposited energy in quartz is given for two ions, Ne at 10 and 100 MeV/amu and Pb at the same velocities. Three points should be underlined. First of all, close to the ion path, more than 10^3 eV nm^{-3} could be transferred to the electronic system (about 40 eV per SiO_2 unit). Secondly the local dose decreases as the inverse square of the radius. Finally, for such ion energies, the radial extent of the energy is larger than 1 μm and depends only on the projectile velocity (2.5 μm at 10 MeV/amu and 10 μm at 100 MeV/amu). We are confident in these results, because their integration over the radius leads to values of the

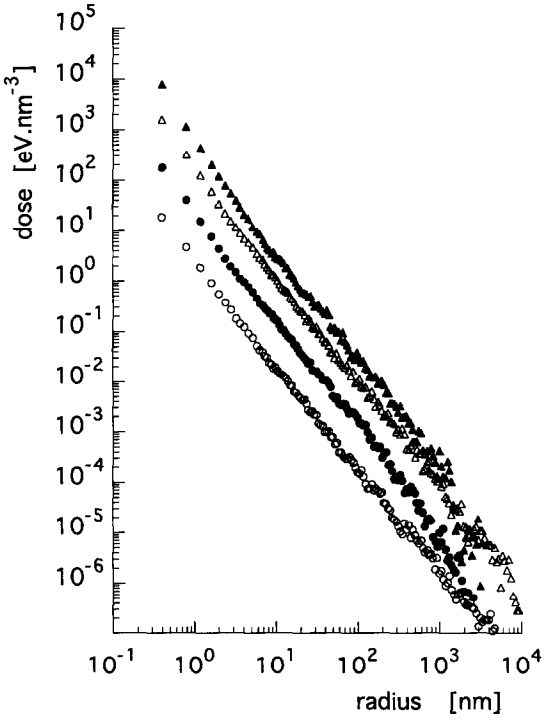

Fig. 1. Deposited energy versus radial distance to the ion path for Ne at 10 and 100 MeV/amu and for Pb at the same velocities in quartz. (▲: Pb 10 MeV/amu, △: Pb 100 MeV/amu, ●: Ne 10 MeV/amu, ○: Ne 100 MeV/amu).

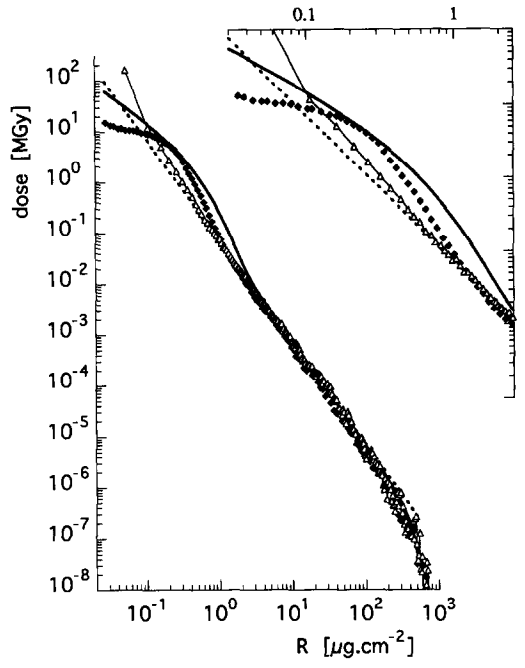

Fig. 2. Comparison of our results for Ne 10 MeV/amu in quartz (△) and graphite (♦) with those of Kieffer (dotted line) and of Waligorski (continuous line).

electronic stopping power close to those given by several authors [4,5] (see Table 3). The cases of 10 MeV/amu Ne in quartz and graphite are compared in Fig. 2 with results already published, those of Kieffer and Straaten [33] and those of Waligorski et al. [34]. These authors give analytical formulae for the radial distribution of the dose, which only depend on the density of the target and on the charge and velocity of the projectiles. Therefore they obtain a universal curve of dose versus the radius R expressed in units of μg cm^{-2}. In every case these curves show approximately a R^{-2} dependence. For the quartz our results are very close to those of Kieffer and Straaten [33] or of Vidiella et al. [54]. A difference only occurs for small distances (smaller than 10 nm), and may be explained by the differences between both calculations. Kieffer's results,

Table 3
The electronic stopping power [eV nm^{-1}] for some ions in quartz given by different authors

Author	Ne 10 MeV/amu	Pb 10 MeV/amu	Ne 100 MeV/amu	Pb 100 MeV/amu
Ziegler [4]	960	26300	150	8700 [a]
Hubert [5]	950	29770	160	9650
MC	1070	27700	170	9700

[a] Values obtained using the Bethe formulae.

which concern the biological matter, are obtained using the binary encounter theory for free electrons. Thus the atom excitation energy due to the creation of holes is not taken into account whereas it is in our calculation (see Figs. 6 and 7). For the quartz, and for a radius smaller than 10 $\mu g\ cm^{-2}$ there is a disagreement between Waligorski's results and ours (and those of Kieffer). This difference comes from the fact that Waligorski's formula drawn up for water using a MC calculation due to Hamm et al. [55] takes empirically into account the plasmon decay, which explains the better agreement for graphite. In our calculation, the plasmon lifetime is estimated from the plasmon peak width in the curve of energy loss versus energy obtained by optical reflectivity measurement [56]. In such a procedure, the wave number dependence of the lifetime is neglected [42]. This approximation is quite valid as long as we are concerned in average values obtained after a great number of plasmon decays. In fact, the plasmon cross section is at maximum for exchange at small wave number, and thus on the average the plasmon wave number must be small and the optical lifetime must be a suitable fit.

For this calculation every primary and secondary electron has been followed above a cutoff value of 2 eV, and no cutoff time was used. Thus we use here the same criteria as other authors [55]. The influence of this choice has been discussed above in section 4. In order to show the contribution of the plasmons to the delocalization of the deposited energy we have compared both calculations, with and without primary plasmon. What we mean by "without plasmon" is the result obtained by taking into account only the individual collisions between the projectile ion and the electron, and all the secondary events, single or collective. In Fig. 3, the radial dose distribution can be shown for Ne and Pb at 10 MeV/amu in graphite. The greatest difference between both behaviours is the presence of a bump due to the plasmon de-excitation which transports away collectively the energy. The difference between both curves gives the dose deposited by the primary plasmons and is shown in Fig. 4. As shown in Table 2, this deposited energy represents about 30% of the electronic stopping power. The radius of the cylinder inside which the electrons lose their energy due to plasmon decay, i.e. 20 Å, weakly depends on the projectile charge and velocity. It actually depends a bit on the impact parameter b for the plasmon creation, which depends itself on the charge and velocity of the projectile, and more on the plasmon lifetime and on the transport properties of the medium. This cylinder radius may be compared with the Bohr adiabatic impact parameter: $v/\omega \sim 12$ Å.

Beyond the dose deposition the MC calculation allows us to describe level by level the number of holes created in a given level. Results for Ne 10 MeV/amu

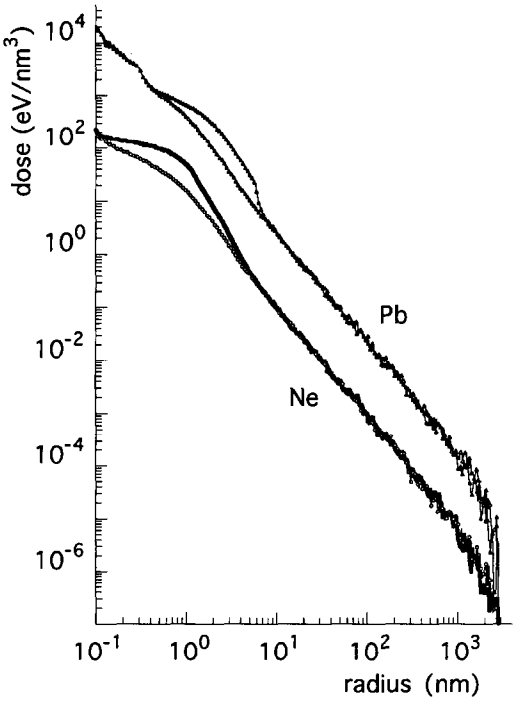

Fig. 3. Deposited energy versus radial distance to the ion path for Ne at 10 MeV/amu and for Pb at the same velocity. For both ions the upper curves include the contribution of the primary plasmons and the lower curves do not.

ions in quartz are reported in Fig. 5. As for the energy deposition, the hole generation may be divided into two contributions, the primary ionisations due directly to ion interactions, and the secondary ones due to the diffusion of the ejected electrons. The ionisations of

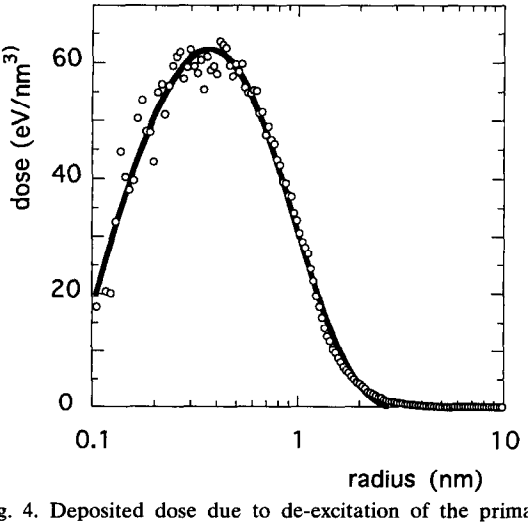

Fig. 4. Deposited dose due to de-excitation of the primary plasmons for Ne 10 MeV/amu in graphite.

deep core levels – with ionisation energy greater than 100 eV – essentially come from ion impacts. Thus the radial distribution of deep ionisation is not as large as the valence hole radial distribution, and it does not have the same shape. For ionisation of core levels, radiative and nonradiative decays should be considered. However, there does not exist any data about the electronic rearrangement of a solid on which multiple core vacancies are generated. The occurrence of such processes could modify the energy distribution because they concern about 25 to 35% of the deposited energy. Although the proportion of core vacancies is small, the energy used to create them could not be neglected. Hence the number of holes generated in the valence band could be significantly modified when Auger processes occur.

The distribution of holes in the valence band approximately follows the same inverse square law as the dose versus radius. In order to obtain the limit of validity of this calculation, we have compared for each level the initial density of electrons with the calculated density of holes. In the case of strong perturbation, Pb at 10 MeV/amu for example, we can show in Fig. 6 that the density of valence holes is overestimated. In

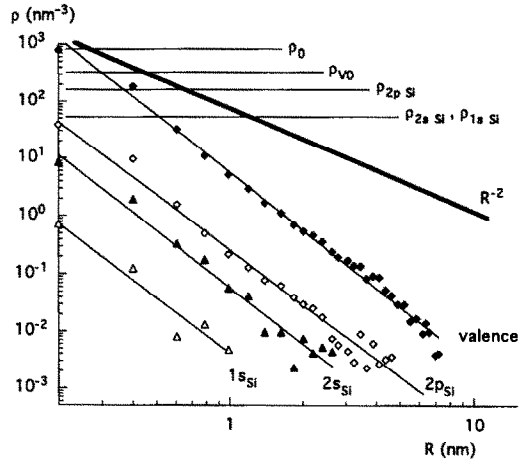

Fig. 6. Density of primary holes created in each level in quartz, for 10 MeV/amu Pb. The thick upper line is the total number of created holes including primaries and secondaries. Each horizontal line indicates the initial average electron density in the shell. ρ_0 is the total electronic density and ρ_{V0} the valence electronic density.

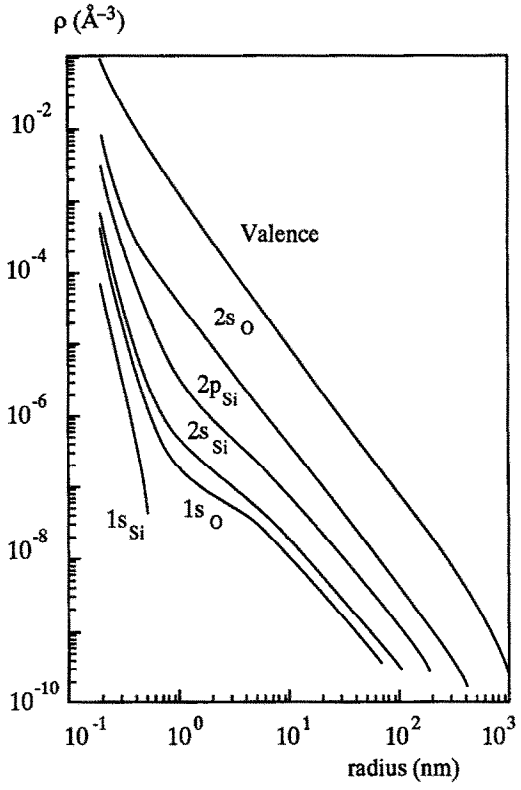

Fig. 5. Density of holes created in each electronic level in quartz for 10 MeV/amu Ne.

fact, within a radius of 0.3 nm the actual number of electrons in the valence band is lower than the amount of ejected valence electrons. Such a discrepancy can be explained by the following considerations. On the one hand, we use a linear theory for both ions and electrons. Such a theory is not accurate enough for the strong perturbations of heavy ions. Moreover the use of a MC method leads us to consider only the interaction of the particle with a medium at equilibrium. So the interactions between excited electrons, which occur for the high density of ionisations predicted by the calculation, cannot be explicitly taken into account. Such interactions should lead to an equipartition of the energy between excited electrons and not directly to supplementary hole creation. On the other hand, the density of primary holes exceeds the initial density too. As expected for intermediate velocities, for which the first Born approximation validity criterion is not fulfilled, the cross section is overestimated. However, the use of such a theory leads to correct values of the stopping power. In fact, any more elaborate calculation of the cross section at intermediate velocity [3] leads to a diminution of the cross section for the same charge state. However, the effective charge state of the projectile should be increased to obtain the right stopping power. This increase with respect to the charge state proposed by Barkas [46] or Hubert et al. [5] agrees qualitatively well with the experiments of stripping for thin foils [48]. Therefore the overestimation of hole density may be explained as follows. Firstly, the impact parameter dependence of the cross sections in a solid

phase is only roughly estimated and some corrections could lead to better results. Secondly a coherent collective mode of interaction could be taken into account for insulators as well as for conductors. Such interactions are efficient to spread out the hole creation far away in the case of graphite, where the primary hole density does not exceed the actual initial density of valence electrons, and it could be the same for insulators even when the lifetime of a plasmon must be shorter.

In spite of these limitations, we can deduce from the hole and electron densities the induced space charge, which is of great interest for the Coulomb explosion model. All the elementary charges are summed up to obtain the overall space charge. The results are shown in Fig. 7 for different times. The space charge is positive inside a small cylinder with a radius of several tenths of a nanometer, and negative elsewhere. Two processes could modify this charge distribution. As mentioned above, the first one is the Auger effect which could contribute to enhance the positive charge around the ion path. The second one is the resulting electric field, which attracts the ejected electrons and could slightly modify their diffusion.

Finally we have calculated the kinetic energy distribution of the electrons for different cutoff times. This result, which is interesting for the thermal spike model, is shown in Fig. 8. These curves present a central peak whose intensity decreases with increasing time, because the energy diffuses outside the core. The part outside the core can be attributed to the fast delta electrons which escape out of it and whose stopping power is smaller than the one of lower energy electrons.

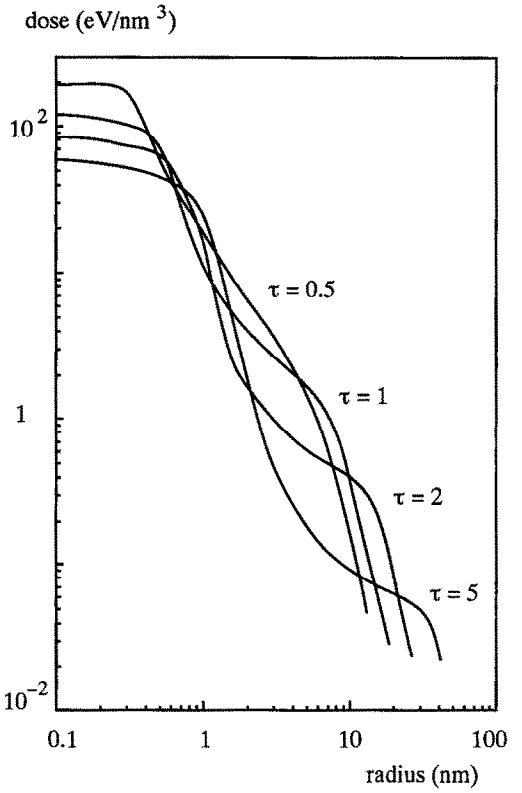

Fig. 8. Time evolution of the kinetic dose versus the radius. τ is the reduced time expressed in units of one plasma period $T = 2\pi/\omega_P \sim 1.7\times10^{-16}$ s.

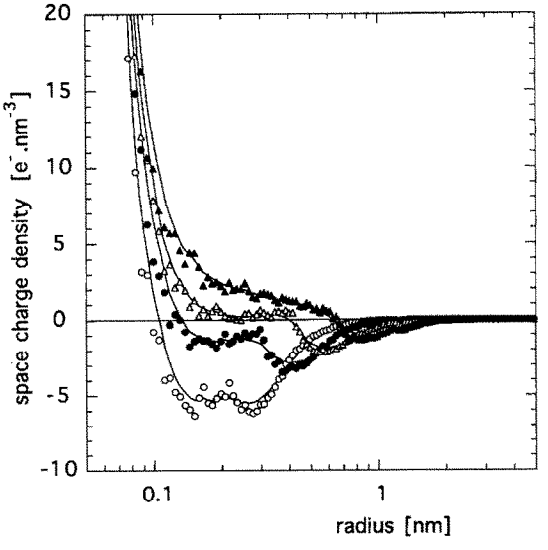

Fig. 7. Time evolution of the space charge density for 10 MeV/amu Ne in graphite. τ is the reduced time expressed in units of one plasma period $T = 2\pi/\omega_P \sim 1.7\times10^{-16}$ s (○: $\tau = 0.5$, ●: $\tau = 1$, △: $\tau = 2$, ▲: $\tau = 5$).

6. Conclusion

We have shown in this paper that the MC method is accurate to give a microscopic description of the ion slowing down effects in the target, since a great number of parameters is explicitly taken into account. Moreover, this code could be easily improved by modifying the interaction cross sections which are the principal input of the numerical treatment. Nevertheless we have to keep in mind that the validity of the MC method is restricted to sufficiently high energy electrons, because of the classical description of the trajectories, and to sufficiently low density of interactions because it cannot take into account nonlinear effects. Besides, the impact parameter estimation we use to deduce the location of the interaction should be improved to obtain a more accurate impact parameter

representation of the cross sections. However, we obtain a precise description of the material excitation, which can be of help for a more comprehensive study of defect creation by ion irradiation.

In addition, the influence of the collective effect has been outlined for both conductor and insulator. So a description which neglects this kind of phenomena could not give a correct quantitative description of the materials modification, particularly for strong perturbations. Moreover, further development should include two other processes: the Auger and radiative decays and the space charge density. Their inclusion needs much more theoretical work, in order to describe the lifetimes and the fluorescence yields for a high density of vacancies created simultaneously inside the solid. For the space charge density a self-consistent calculation which takes into account the induced electric field should be developed. These latter points constitute a challenge for new theoretical descriptions of ion–solid interaction.

References

[1] H. Bethe, Handbuch der Physik, vol. 14 (1933) p. 491.
[2] J. Lindhard, V. Nielsen, M. Scharff and P.V. Thomsen, K. Dan. Vidensk. Selsk. Mat. Fys. Medd. 33 no. 10 (1963).
[3] P.D. Fainstein, V.H. Ponce and R.D. Rivarola, J. Phys. B: At. Mol. Opt. Phys. 21 (1988) 287.
[4] J.F. Ziegler, J.P. Biersack and U. Littmark, The Stopping and Ranges of Ions in Solids, ed. J.F. Ziegler (Pergamon, 1980).
[5] F. Hubert, R. Bimbot and H. Gauvin, Atomic Data and Nucl. Data Tables 46 (1990), 1.
[6] G. Schiewitz, H. Platten, D. Schneider, T. Schneider, W. Zeitz, K. Musiol, R. Kowalik and N. Stolterfoht, Reports of the Hahn–Meitner Institut (October 1987).
[7] R. Spohr, Ion Tracks and Microtechnology (Vieweg, Braunschweig, 1990).
[8] P.M. Echenique, F. Flores and R.H. Ritchie, Solid State Physics 43 (1990) 229.
[9] D.A. Young, Nature 182 (1958) 375.
[10] R.L. Fleisher, P.B. Price and R.M. Walker, Nuclear Tracks in Solids: Principles and Applications (University of California Press, 1975).
[11] S.A. Durrani and R.K. Bull, Solid State Nuclear Track Detection (Pergamon, Oxford, 1987).
[12] E. Dartyge, J.P. Duraud, Y. Langevin and M. Maurette, Phys. Rev. B 23 (1981) 5213.
[13] D. Albrecht, E. Balanzat and K. Schaupert, Nucl. Tracks Radiat. Meas. 11 (1986) 93.
[14] F. Studer, C. Houpert, H. Pascard, R. Spohr, J. Vetter, Jin Yun Fan and M. Toulemonde, Radiat. Eff. and Defects in Solids 116 (1991) 59.
[15] M. Toulemonde and F. Studer, Solid State Phenomena 30/31 (1993) 477.
[16] E. Balanzat, Radiat. Eff. and Defects in Solids 126 (1993) 97.
[17] A. Dunlop, D. Lesueur, P. Legrand, H. Dammak, and J. Dural, Proc. 15th Int. Conf. on Atomic Collisions in Solids, London, Ontario, Canada, 1993, Nucl. Instr. and Meth. B 90 (1994) 330.
[18] C. Dufour, A. Audouard, F. Beuneu, J. Dural, J.P. Girard, A. Hairie, M. Levallois, E. Paumier and M. Toulemonde, J. Phys. Condensed Matter 5 (1993) 4575.
[19] A. Dunlop and D. Lesueur, Radiat. Eff. and Defects in Solids 126 (1993) 123.
[20] V. Hardy, D. Groult, M. Hervieu, J. Provost, B. Raveau and S. Bouffard, Nucl. Instr. and Meth. B 54 (1991) 472.
[21] F. Rullier-Albenque, A. Legris, S. Bouffard, E. Paumier and P. Lejay, Physica C 175 (1991) 111.
[22] A. Audouard, E. Balanzat, S. Bouffard, J.C. Jousset, A. Chamberod, A. Dunlop, D. Lesueur, G. Fuchs, R. Spohr, J. Vetter and L. Thomé, Phys. Rev. Lett. 65 (1990) 875.
[23] A. Benyagoub and S. Klaumünzer, Radiat. Eff. and Defects in Solids 126 (1993) 105.
[24] F. Seitz and J.F. Koehler, Solid State Phys. 2 (1956) 305.
[25] M. Toulemonde, C. Dufour and E. Paumier, Phys. Rev. B 46 (1992) 14362.
[26] C. Dufour, A. Audouard, F. Beuneu, J. Dural, J.P. Girard, A. Hairie, M. Levallois, E. Paumier and M. Toulemonde, J. Phys.: Condensed Matter 5 (1993) 4573.
[27] D. Lesueur and A. Dunlop, Radiat. Eff. and Defects in Solids 126 (1993) 163.
[28] C.L. Wingate and J.W. Baum, Radiation Research 65 (1976) 1.
[29] M.N. Varma and J.W. Baum, Radiation Research 81 (1980) 355.
[30] E.J. Kobetitch and R. Katz, Phys. Rev. 170 (1968) 391.
[31] J. Fain, M. Monnin and M. Montret, Radiation Research 57 (1974) 379.
[32] M. Zaider, D.J. Brenner and W.E. Wilson, Radiation Research 95 (1983) 231.
[33] J. Kieffer and H. Straaten Phys. Med. Biol. 31, no. 11 (1986) 1201.
[34] M.P.R. Waligorski, R.N. Hamm and R. Katz, Nucl. Track. Radiat. Meas. 11 (1986) 309.
[35] G. Kraft, M. Kramer and M. Scholz, Radiat. Environm. Biophysics.
[36] R.A. Sparrow, R.E. Olson and D. Scneider, J. Phys. B: At. Mol. Opt. Phys. 25 (1992) 1295.
[37] E. Tosatti, Interaction of radiation with condensed matter, vol. I (IAEA, Vienna, 1977) p. 295.
[38] J. Lindhard, K. Dan. Vidensk. Selsk. Mat. Fys. Medd. 28 (1954) 1.
[39] R.H. Ritchie and V.E. Anderson, IEEE Trans. Nucl. SCI. NS-18 (1971) 141.
[40] W. Brandt and J. Reinheimer, Phys. Rev. B 2 (1970) 3104.
[41] M. Rössler and W. Brauer, Phys. Status Solidi B 104 (1981) 161.
[42] H. Raether, Excitation of Plasmons and Interband Transitions by Electrons (Springer, 1980).
[43] W. Bambynek, B. Crasemann, R.W. Fink, H.U. Freund, H. Mark, C.D. Swift, R.E. Price and P. Venugopala Rao, Rev. Mod. Phys. 44 (1972) 716.
[44] M.O. Krause, J. Phys Chem. Ref. Data 8 (1979) 307.
[45] E.J. McGuire, Phys. Rev. A 3 (1971) 1801.
[46] H. Barkas, Nucl. Res. Emulsions, vol. 1 (Academic Press, (1963) p. 371.

[47] A. Cassimi, J.P. Grandin and M.G. Suraud, Suppl. Z. Phys. D 21 (1991) 329.
[48] G.S. Khandelwal and E. Merzbacher, Phys. Rev. 151 (1966) 12.
[49] G.S. Khandelwal and E. Merzbacher, Atomic Data 1 (1969), 103.
[50] V.J. Johnson, Properties of materials at low temperatures, A Compendium (Pergamon, 1961).
[51] G. Moliere, Z. Naturforschung A 2 (1947) 133.
[52] M. Gryzinski, Phys. Rev. 138 (1965) A 305; Phys. Rev. 138 (1965) A 322; Phys. Rev. 138 (1965) A 336.
[53] L. Douillard, E. Doorhyee, J.P. Duraud, F. Jollet and R.A.B. Devine, Radiat. Eff. and Defects in Solids 126 (1993) 237.
[54] G. Vidiella, Y. Patin and A. Touati, Annales de Phys., Col. no. 2, Supp. no. 6, 14 (1989) 51.
[55] R.N. Hamm, J.E. Turner, R.H. Ritchie and H.A. Wright, Radiation Research, Suppl. 8, 104 (1986) 20.
[56] E.A. Taft and H.R. Philipp, Phys. Rev. 138 (1965) A 197.